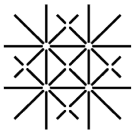

University of Basel

Violating the thermodynamic uncertainty relation in the three-level laser driven by a thermal bath and an external field

Master-Thesis

Sander Stammbach
Prof. Patrick Potts
Dr. Mateo Brunelli
Marcelo Janovitch

2023

1 Todo

1. read through the hole that, checkloutline, and look, if everything is consistent
2. TUR Plot 2*6
3. jh, p und jcav von high f approx in unterkapitel eqm plot aber dort lassen
4. Moment generating function

2 Acknowledgements

The completion of my master's thesis was made possible through the consistent support and guidance generously provided by my supervisor, Prof. Patrick Potts. His direct yet compassionate approach not only navigated me through the diverse challenges of my master's thesis but also made the journey thoroughly gratifying, culminating in its successful completion. I express immense gratitude for his invaluable support. Special thanks are also due to Matteo Brunelli and Marcelo Janovitch, who not only supervised my master's project but also provided invaluable assistance and guidance with technical intricacies throughout the entire process. Furthermore, I extend my gratitude to Marcelo Janovitch for engaging in helping me many times to improve my writing, offering insightful references relevant to the topics covered in my thesis, and warmly welcoming further exploration and exchange of ideas. Their contributions were immensely appreciated and significantly enriched the depth of my research. I would like to express my sincere appreciation to all mentioned for their unwavering support, guidance, and scholarly camaraderie throughout this academic journey.

Contents

1 Todo **1**

2 Acknowledgements **1**

3 Introduction **3**

4 System and Model **4**
4.1 Rotating frame 6

5 Equations of motion **6**
5.1 Factorization 6
5.2 Approximation for high external field strength f 7
5.3 Heat current versus external field 7

6 Laws of thermodynamic **8**
6.1 First law of thermodynamic 8
6.1.1 Equations of motion 9
6.2 Second law 10

7 Double threshold behavior and population inversion **12**
7.1 Wigner functions for different temperatures 13

8 Influence of the external field **15**
8.1 Photocurrent and Power 15
8.2 Non-linear behavior from the field 15
8.3 Wigner function as a function of external field strength, f 16

9 Fluctuation theory **18**
9.1 Thermodynamic Uncertainty Relation 18
9.2 Full counting statistics 18
9.3 Violating the TUR 20

10 Conclusion **23**

A Rotating frame transformation **24**

B Equation of motion **25**

C Full counting statistics **26**
C.1 Vectorisation 27

D bullet points **27**

3 Introduction

Heat engines have been of interest since the industrialization period. The concept involves converting thermal energy into kinetic energy, which can then be utilized. The concept of converting thermal energy was adopted from (Scovil and Schulz [9] and applied to a 3-level quantum system. However, in this case, the energy output is a state of light wave. In other words, it is possible to build a maser that is driven by the interaction with a hot and cold reservoir. This study analyzed a modified form of such a three-level maser. The modification compared to the original version is that this three-level system is placed in a cavity and can be driven by an external field. To gain as much knowledge as possible about this quantum heat engine, various aspects are discussed in this thesis. It should be noted that the calculations were performed both analytically using the equations of motion and numerically. One focus was on analyzing the heat flow and its behavior when parameters change. This revealed phenomena that can only be explained quantum mechanically, such as the double-threshold behavior which is described in [6]. The question that arises and we investigate is how the external field affects the system and changes the photocurrent and power. We also investigated the non-linear behavior of the expected value of $\langle a \rangle$ and compared it to the analytical solution outlined in Aufleres' paper [2].

To further understand the heat flow or heat current J, we also discuss the thermodynamic uncertainty relation (TUR) as in [4]. We examine thermodynamic uncertainty in detail in the three-level maser and find coherence-induced TUR violations. TUR violation allows us to identify operating regimes where quantum dynamics lead to improved performance quantified by a lower value of the TUR as the classical limit. Interestingly, such a quantum advantage cannot be expected from the off-diagonal elements of the density matrix alone, as fluctuations are not solely encoded in the steady-state coherence. We investigated all the parameters that describe our 3-level maser and found an optimum where TUR violation exists. Similar to the work by [4], our three-level system is also coupled to a hot and cold bath. Additionally, it is driven by an external field. In comparison to [4] approach, the three-level system is situated within a cavity. This results in a complete transformation of the state of light, as well as a change in the circumstances under which the thermodynamic imbalance relation (TUR) is violated.

H

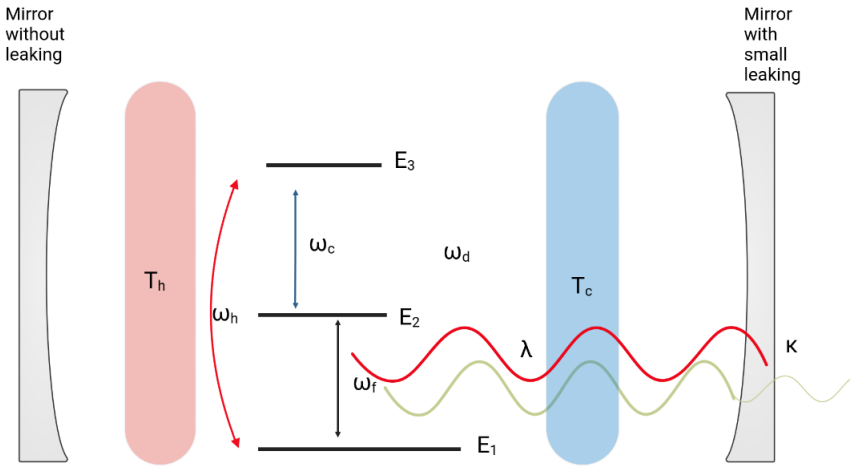

Figure 1: Schematic representation of our three-level laser continuously coupled to two reservoirs of temperatures T_h and T_c. The three energy levels are described by the eigenenergies E_1, E_2, E_3. The system is interacting with a quantized single-mode field. λ represents the strength of matter-field coupling. The ω_h, ω_c, ω_f describe the transition frequencies. The frequency of the drive field is ω_d, shown with a red line.

4 System and Model

A laser produces coherent light, which means all the photons that the laser produces, have the same phase and frequency. The three essential elements of a laser are the gain medium, the pump source, and the cavity, also known as an optical resonator.

The gain medium is a material capable of generating and amplifying light. It consists often of material that allows atomic transitions. The gain medium contains at least a three-level system in an excited state and is further excited by the pump mechanism.

The pumping mechanism provides the energy to bring the atoms or molecules in the active medium to the excited state. The energy input causes the atoms or molecules to move to a higher energy state. In our case, it is a thermal bath and an external field.

The cavity consists of two mirrors that reflect and amplify the light inside the laser. One of the mirrors is partially transparent to let some of the light out as a laser beam. The resonator creates feedback of the light to be reflected back and forth between the mirrors and amplified in the process [8].

If the atomic state is in the highest state, we talk about excited states. Population inversion is a term describing the situation while a system exists in a state in which more members of the system are in excited states. Thus, the pump energy is stored and a population inversion can be built up. Through stimulated emission by a photon, a second coherent photon will be emitted. This light has the same wavelength and phase as the incident light and further amplifies it. The excited state decays back into the ground state again and the cycle can start all over again. To increase the probability that a photon will produce a stimulated photon, the photon must pass through the gain medium several times. Therefore, the laser medium is embedded in a cavity, whereby the photons are reflected forth. Feedback in the cavity causes the light to be amplified repeatedly, resulting in an intense, coherent laser beam. These mirrors also finally determine the direction of the generated light beam. One of the two mirrors is designed to be partially transparent so that part of the light can escape and be directed to its use [6].

Throughout this thesis, we consider a three-level system with energies E_1, E_2, and E_3, embedded in a cavity with frequency ω_{cav}, shown in Fig 1 For future reference, we introduce the transition frequencies: $(E_3 - E_1) = \omega_h$, $(E_3 - E_2) = \omega_c$ and the transition $(E_2 - E_1) = \omega_f$ which interacts with the cavity, where $\hbar = 1$ The Hamiltonian which describes the energy of the three-level system and the cavity mode, without

interaction, can be written as follows,

$$H_{free} = \sum_{\alpha=1}^{3} E_i \left|i\right\rangle\!\left\langle i\right| + \omega_{cav} a^\dagger a, \tag{1}$$

where α describes the three different states. The bosonic ladder operators are a and $a^\dagger$ with the commutation relations:$[a, a] = [a^\dagger, a^\dagger] = 0$ and $[a, a^\dagger] = 1$. Our cavity is in resonance with the transition frequency between the states $|1\rangle$ and $|2\rangle$, therefore we set $\omega_{cav} = \omega_f$.

We consider the cavity to be coherently driven with frequency ω_d, to introduce a phase we apply a coherent external field [4]. The strength of the external field is described by f Described by the Hamiltonian

$$V = f(e^{-i\omega_d t} a^\dagger + e^{i\omega_d t} a). \tag{2}$$

A Jaynes-Cummings Hamiltonian models the coupling between the photons and the three-level system,

$$H_{int} = g(\sigma_{12} a^\dagger + \sigma_{21} a), \tag{3}$$

where $\sigma_{12} = |1\rangle\langle 2|$ and $\sigma_{21} = |2\rangle\langle 1|$ are the transition operators. The coupling constant g describes the interaction between the system and the photons in the cavity.

The total Hamiltonian is the sum of (1) (3), (2),

$$H_{tot} = H_{free} + H_{int} + V. \tag{4}$$

To describe the open system dynamics, we introduce the density matrix. The complete description of the system's state at a given time t is encoded in the density matrix $\rho(t)$ [6]. Its time-evolution is determined by the master equation

$$\dot{\rho}(t) = \frac{1}{i}[H, \rho] + \mathcal{L}_h \rho + \mathcal{L}_c \rho + \mathcal{L}_{cav} \rho. \tag{5}$$

The first part of eq.(5) describes unitary time-evolution due to the Hamiltonian. The interaction with the various environmental heat baths is described by the non-unitary part. Open system evolution doesn't conserve purity

$$\begin{aligned} \mathcal{L}_h \rho &= \frac{\gamma_h}{2}(n_h + 1)\mathcal{D}[\sigma_{13}]\rho + \frac{\gamma_h}{2} n_h \mathcal{D}[\sigma_{31}]\rho, \\ \mathcal{L}_c \rho &= \frac{\gamma_c}{2}(n_c + 1)\mathcal{D}[\sigma_{23}]\rho + \frac{\gamma_c}{2} n_c \mathcal{D}[\sigma_{32}]\rho, \\ \mathcal{L}_{cav} \rho &= \kappa(n_{cav} + 1)\mathcal{D}[a]\rho + \kappa n_{cav} \mathcal{D}[a^\dagger]\rho. \end{aligned} \tag{6}$$

The coupling of the system and the hot bath is described by $\mathcal{L}_h$, $\mathcal{L}_c$ is the contribution from the coupling with the cold bath coupled with the atom. The loss and gain of the photons that are in the cavity, due to finite temperature are described by $\mathcal{L}_{cav}$. Where

$$\mathcal{D}[A]\rho = (2A\rho A^\dagger - A^\dagger A \rho - \rho A^\dagger A). \tag{7}$$

The mean number of photons in the reservoirs is determined by the Bose-Einstein distribution

$$n_\alpha = \frac{1}{\exp\left[\frac{\omega_\alpha}{k_b T_\alpha}\right] - 1}, \tag{8}$$

The prefactor γ_c, γ_h, κ describe the spontaneous decay rates.

The working principle of the three-level laser may be understood by considering the following cycle. First, the system is pumped, by the hot bath, from the lowest E_1 level to the highest level E_3. From state E_3 the system decays to the lower state E_2 by emitting a photon into the cold bath. From E_2 the decay of the system comes through the stimulated emission of a photon, into the lowest state E_1. This cycle repeats itself over and over again and is driven by the thermal gradient between the hot (T_h) and the cold (T_c) bath. As described in 1 The incoming field is also crucial for the heat flow. Through stimulated emission, it ensures that photons decay from P_2 to P_1. Thus the external field pushes the cycle on

4.1 Rotating frame

In thermodynamics, we are often interested in the long-time limit. Therefore the calculations could be done in steady states. The rotating frame is a reference frame that rotates at the frequency of the driving field, allowing for a simplified analysis of the system dynamics. The rotating frame Approximation is a quantum mechanics technique that transforms a system's Hamiltonian into a rotating reference frame, extracting the time-dependent phase factor and simplifying equations. This allows for a more direct analysis of system dynamics in numerical calculations by eliminating time-dependent terms. In our case, the aim was to remove the time-dependent term of the external excitation field of V (2). This method proves particularly useful when the system exhibits rapid oscillations or precession around a specific axis. The derivation of the master-equation in the rotating frame is shown in the appendix (59). The transformation is done with the unitary

$$U = \exp\big(-it(\omega_d a^\dagger a + E_1 |1\rangle\langle 1| + (E_1 + \omega_d) |2\rangle\langle 2| + E_3 |3\rangle\langle 3|)\big). \tag{9}$$

The derivation can be found in the appendix A. The new master equation is

$$\dot{\rho_I}(t) = \frac{1}{i}[H_I, \rho_I] + \mathcal{L}_h \rho_I + \mathcal{L}_c \rho_I + \mathcal{L}_{cav} \rho_I, \tag{10}$$

where $\rho_I = U^\dagger \rho U$ is the density matrix of the system in the rotating frame. The total Hamiltonian in the rotating frame H_I is an ingredient in the master equation in the rotating frame(10). With the detuning $\Delta_1 = \omega_{cav} - \omega_d$ and $\Delta_2 = (E_2 - (E_1 + \omega_d))$. The transformed Hamiltonian can be rewritten as,

$$H_I = H_{int} + f(a^\dagger + a) + \Delta_1 a^\dagger a + \Delta_2 |2\rangle\langle 2|. \tag{11}$$

5 Equations of motion

In a three-level system, the equation of motion can be described in a rotating frame.

We study the system dynamics through the Heisenberg equations of motion. We understand the averages of the different time derivatives of the relevant operators $\mathcal{O}$. The equation of motion for the density matrix elements in the rotating frame can be calculated as $\partial_t \langle \mathcal{O} \rangle = -i \operatorname{Tr}\{[H_I, \mathcal{O}]\rho\} + \operatorname{Tr}\{\mathcal{O}\mathcal{L}\rho\}$ Solving the equation of motion in the rotating frame allows for the analysis of the dynamics of the three-level maser system, including the average of the population inversion, the transition operator, and the emission of coherent radiation. The averages of the different time derivatives of the relevant operators are presented in the set of equations below.

$$\partial_t \langle a \rangle = -i(g\langle \sigma_{12} \rangle + \Delta_1 \langle a \rangle + f) - \kappa \langle a \rangle, \tag{12}$$

$$\partial_t \langle p_2 \rangle = -ig(\langle \sigma_{21} a \rangle - \langle \sigma_{12} a^\dagger \rangle) + \gamma_c((n_c + 1)(1 - \langle p_2 + p_1 \rangle) - n_c \langle p_2 \rangle), \tag{13}$$

$$\partial_t \langle p_1 \rangle = -ig(\langle \sigma_{12} a^\dagger \rangle - \langle \sigma_{21} a \rangle) + \gamma_h((n_h + 1)(1 - \langle p_2 + p_1 \rangle) - n_h \langle p_1 \rangle), \tag{14}$$

$$\begin{aligned} \partial_t \langle \sigma_{12} a^\dagger \rangle = {} & i(g(\langle p_2 \rangle + \langle (p_2 - p_1) a^\dagger a \rangle) + f\langle \sigma_{12} \rangle + \Delta_1 \langle \sigma_{12} a^\dagger \rangle - \Delta_2 \langle \sigma_{12} a^\dagger \rangle) \\ & - \frac{\gamma_h}{2} n_h \langle \sigma_{12} a^\dagger \rangle - \frac{\gamma_c}{2} n_c \langle \sigma_{12} a^\dagger \rangle - \kappa \langle \sigma_{12} a^\dagger \rangle, \end{aligned} \tag{15}$$

$$\partial_t \langle \sigma_{12} \rangle = -ig(\langle (p_1 - p_2) a \rangle) - \frac{\gamma_c}{2} n_c \langle \sigma_{12} \rangle - \hbar \frac{\gamma_h}{2} n_h \langle \sigma_{12} \rangle, \tag{16}$$

$$\partial_t \langle a^\dagger a \rangle = -i(g(\langle \sigma_{12} a^\dagger \rangle - \langle \sigma_{21} a \rangle) + f(\langle a^\dagger \rangle - \langle a \rangle)) + 2\kappa(n_{cav} - \langle a^\dagger a \rangle). \tag{17}$$

5.1 Factorization

To solve the equations of motion we make an approximation and factorize the $\langle p_1 a^\dagger a \rangle$ and $\langle p_2 a^\dagger a \rangle$ to $\langle p_1 \rangle \langle a^\dagger a \rangle$ and $\langle p_2 \rangle \langle a^\dagger a \rangle$.And $\langle p_1 a \rangle$ to$\langle p_1 \rangle \langle a \rangle$. The same thing is done for $\langle a^\dagger \rangle$ and $\langle p_2 \rangle$.

In the case of steady states, where we anticipate that all time derivatives on the left-hand side of the equations are zero, we can resolve them. Described in the appendix (67) and (68) give zero, therefore we can cancel (18), (22) and (24). The separation of the real and the imaginary parts of those equations gives the equations:

$$\partial_t \mathrm{Im}[\langle a\rangle] = -g\mathrm{Re}[\langle\sigma_{12}\rangle] - f - \kappa\mathrm{Im}[\langle a\rangle], \tag{18}$$

$$\partial_t \mathrm{Re}[\langle a\rangle] = g\mathrm{Im}[\langle\sigma_{12}\rangle] - \kappa\mathrm{Re}[\langle a\rangle], \tag{19}$$

$$\partial_t\langle p_2\rangle = -2g(\mathrm{Im}[\langle\sigma_{12}a^\dagger\rangle]) + \gamma_c((n_c+1)(1-\langle p_2+p_1\rangle) - n_c\langle p_2\rangle), \tag{20}$$

$$\partial_t\langle p_1\rangle = 2g(\mathrm{Im}[\langle\sigma_{12}a^\dagger\rangle]) + \gamma_h((n_h+1)(1-\langle p_2+p_1\rangle) - n_h\langle p_1\rangle), \tag{21}$$

$$\begin{aligned}\partial_t \mathrm{Im}[\langle\sigma_{12}a^\dagger\rangle] = g(\langle p_2\rangle + \langle(p_2-p_1)\rangle\langle a^\dagger a\rangle) - f\mathrm{Re}[\langle\sigma_{12}\rangle] \\ - \frac{\gamma_h}{2}n_h\mathrm{Im}[\langle\sigma_{12}a^\dagger\rangle] - \frac{\gamma_c}{2}n_c\mathrm{Im}[\langle\sigma_{12}a^\dagger\rangle] - \kappa\mathrm{Im}[\langle\sigma_{12}a^\dagger\rangle],\end{aligned} \tag{22}$$

$$\partial_t \mathrm{Re}[\langle\sigma_{12}a^\dagger\rangle] = f\mathrm{Im}[\langle\sigma_{12}\rangle] - \frac{\gamma_h}{2}n_h\mathrm{Re}[\langle\sigma_{12}a^\dagger\rangle] - \frac{\gamma_c}{2}n_c\mathrm{Re}[\langle\sigma_{12}a^\dagger\rangle] - \kappa\mathrm{Re}[\langle\sigma_{12}a^\dagger\rangle], \tag{23}$$

$$\partial_t \mathrm{Im}[\langle\sigma_{12}\rangle] = -g(\langle(p_1-p_2)\rangle\mathrm{Re}[\langle a\rangle]) - \frac{\gamma_c}{2}n_c\mathrm{Im}[\langle\sigma_{12}\rangle] - \frac{\gamma_h}{2}n_h\mathrm{Im}[\langle\sigma_{12}\rangle], \tag{24}$$

$$\partial_t \mathrm{Re}[\langle\sigma_{12}\rangle] = g(\langle(p_1-p_2)\rangle\mathrm{Im}[\langle a\rangle]) - \frac{\gamma_c}{2}n_c\mathrm{Re}[\langle\sigma_{12}\rangle] - \frac{\gamma_h}{2}n_h\mathrm{Re}[\langle\sigma_{12}\rangle], \tag{25}$$

$$\partial_t\langle a^\dagger a\rangle = 2g(\mathrm{Im}[\langle\sigma_{12}a^\dagger\rangle] + 2f\mathrm{Re}[\langle a\rangle] + 2\kappa(n_{cav} - \langle a^\dagger a\rangle) \tag{26}$$

5.2 Approximation for high external field strength f

To better complain our work with [4], we are looking for a high f limit for the occupation number and the photon number. For that, we make the approximation. If the external field f is big compers to the coupling constant g and the impact of g is negligible, we conclude out of 18 the approximation , $\langle a\rangle = -\frac{-if}{\kappa}$. Out of the equations of motions (20),(21),(24),(25) we derive the approximated equations of motions for the expectation of the occupation probabilities,

$$\langle p_1\rangle = \frac{\gamma_c\gamma_h\kappa^2 n_c(1+n_h)(\gamma_c n_c+\gamma_h n_h) + 4f^2g^2(\gamma_c+\gamma_h+\gamma_c n_c+\gamma_h n_h)}{\gamma_c\gamma_h\kappa^2(\gamma_c n_c+\gamma_h n_h)(n_c+n_h+3n_c n_h) + 4f^2g^2(\gamma_c(2+3n_c)+\gamma_h(2+3n_h))}, \tag{27}$$

and

$$\langle p_2\rangle = \frac{\gamma_c\gamma_h\kappa^2(1+n_c)n_h(\gamma_c n_c+\gamma_h n_h) + 4f^2g^2(\gamma_c+\gamma_h+\gamma_c n_c+\gamma_h n_h)}{\gamma_c\gamma_h\kappa^2(\gamma_c n_c+\gamma_h n_h)(n_c+n_h+3n_c n_h) + 4f^2g^2(\gamma_c(2+3n_c)+\gamma_h(2+3n_h))}. \tag{28}$$

For the average of $\mathrm{Re}[\langle\sigma_{12}\rangle]$ we get,

$$\mathrm{Re}[\sigma_{12}] = \frac{2fg(n_h-n_c)\gamma_c\gamma_h\kappa}{4f^2g^2((2+3n_c)\gamma_c+(2+3n_h)\gamma_h) + (n_c+n_h+3n_c n_h)\gamma_c\gamma_h(n_c\gamma_c+n_h\gamma_h)\kappa^2}. \tag{29}$$

Out of the approximated occupation probabilities and the approximated σ_{12}it is possible to express the heat currents as well as the photocurrent and power. This will be done in section 6.1.1.

5.3 Heat current versus external field

We now have three calculation methods available. Firstly, we can numerically solve the master equation. Secondly, we can numerically solve the expected values of the equations of motion. Alternatively, we can utilize the purely analytical solutions of the high f approximation. To compare the three different calculation methods with each other we can have a look at fig 2 for the current versus the external field To plot the power, the calculations are done as in (36) against different values of f and is shown in Fig. 2.

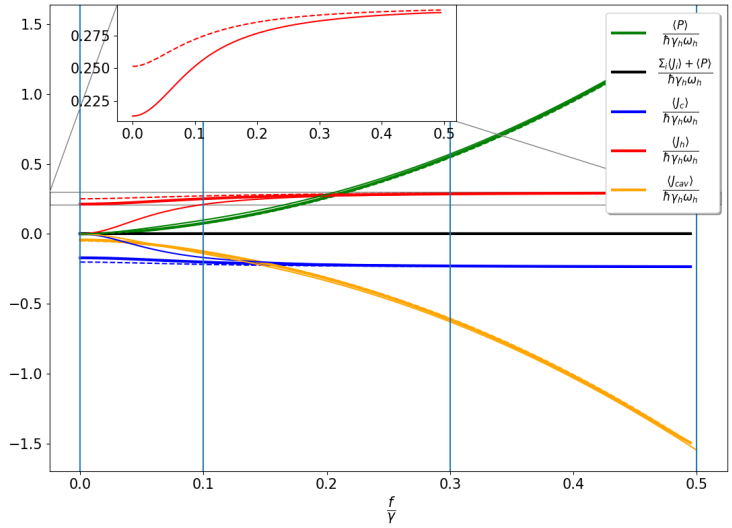

Figure 2: The heat currents are calculated with equations (33)-(35) and the power (36) are calculated against different external field strength f. With thick solid lines, the numerical calculations of the master equation are visualized. The high f approximation is shown with thin solid lines Dashed lines show the numerical solution of the equations of motion. The temperature $n_h = 11$ is set to the maximum in entropy production. The parameters for the system are, expressed with the decay rates $\gamma = 1$. The values for all the relevant parameters in the system are $\gamma_c = \gamma_h = \gamma = 1, g = 14\kappa, \omega_{cav} = 30\gamma, \omega_h = 150\gamma, \omega_c = 120\gamma, n_h = 11, n_c = n_{cav} = 0.01, \kappa = 0.2\gamma$. The blue horizontal line marks the values of f, for which the Wigner functions are visualized in 10.

The fact that the calculations match the results from the numerical calculations confirms the results of the equations of motion. Here, the behavior of heat current, the photocurrent, and the power as functions of the strength of the external field strength f are examined. Upon observing the heat current J_h in the heat in the fig. 2, it is immediately noticeable that its magnitude remains constant when the temperature is around ($n_h = 11$). For the photon current and power, a quadratic increase is observed, consistent with the findings in the high-f approximation (40). At high temperatures, ($n_h = 100$) occurs after the peak of the Double-Threshold Behavior 7, and the influence of f on the heat flow is evident. For the behavior of heat flow at very low temperatures, reference is made to the section "Non-linear Behavior," where a cubic increase in heat flow is demonstrated in 8.2.

6 Laws of thermodynamic

6.1 First law of thermodynamic

According to the first law of thermodynamics, the change in internal energy of a closed system is equal to the sum of the change in heat and the change in work. This is illustrated through a graphical representation 3 where the combined values of heat currents and power are plotted. It is noteworthy that their sum converges to zero, fulfilling the first law of thermodynamics. 2,3, and 5. The first law of thermodynamics could be represented by the following equation

$$\Delta U = \Delta Q + \Delta W. \tag{30}$$

Where U is the internal energy, Q is the heat, and W is the work. To calculate the internal energy, H_{free} is considered, see lecture [7]. In quantum mechanics, the equation can be rewritten as

$$\partial t\langle H_{free}\rangle = -i\,\mathrm{Tr}\{[H_{free}, H_I]\rho_I\} + \mathrm{Tr}\{\sum_i (H_{free}\mathcal{L}_i\rho_I)\}. \tag{31}$$

What we get is

$$\partial t\langle H_{free}\rangle = \langle P\rangle + \langle J_h\rangle + \langle J_c\rangle + \langle J_{cav}\rangle. \tag{32}$$

To calculate the average heat flow we can take the trace from $\mathrm{Tr}\{\mathrm{H}_{\mathrm{free}}\mathcal{L}\rho\}$. where the results for the different currents are

$$\langle J_h\rangle = \mathrm{Tr}\{H_{free}\mathcal{L}_h\rho\} = \omega_h\gamma_h((n_h)P_1 - (n_h+1)P_3). \tag{33}$$

The same calculation can be done for the interaction with the cold bath.

$$\langle J_c\rangle = \mathrm{Tr}\{H_{free}\mathcal{L}_c\rho\} = \omega_c\gamma_c((n_c)P_2 - (n_c+1)P_3). \tag{34}$$

For the calculation the $\mathrm{Tr}\{H_{free}\mathcal{L}_{cav}\}$, The result for the photocurrent is

$$\langle J_{cav}\rangle = \mathrm{Tr}\{H_{free}\mathcal{L}_{cav}\rho\} = 2\omega_{cav}\kappa(n_{cav} - \langle a^\dagger a\rangle). \tag{35}$$

J_h is an energy input in the system, therefore it has another singe as J_c, J_{cav}.

As in Fig 2 we look for $\langle J_i\rangle$ on different driving constants f. In other words, in the figure, the Trace from the density matrices times the Liouvilian against the drive strength is visualized. For the average power, we get

$$\langle P\rangle = -i\mathrm{Tr}\{H_{free}[H_I,\rho_I]\} = -i\omega_{cav}f(\langle a^\dagger\rangle - \langle a\rangle). \tag{36}$$

To get the heat current out of the equations of motion, we expressed them with the formulas of the occupation probability. The power is expressed with $P = -2f\omega_{cav}\mathrm{Im}[\langle a\rangle]$.

6.1.1 Equations of motion

In this section, the equations of motion are proved, if they yield the first law of thermodynamics. The heat currents, the photon current, and the power can be described with the formulas (36) -(33) and plugged into the equations of motion.

$$\frac{\langle J_h\rangle}{\omega_h} = -ig(\langle\sigma_{12}a^\dagger\rangle - \langle\sigma_{21}a\rangle) = \omega_h\frac{2gf\mathrm{Im}[\sigma_21]}{\kappa} \tag{37}$$

$$\frac{\langle J_c\rangle}{\omega_c} = ig(\langle\sigma_{12}a^\dagger\rangle - \langle\sigma_{21}a\rangle) = -\omega_c\frac{2gf\mathrm{Im}[\sigma_21]}{\kappa} \tag{38}$$

$$\frac{\langle J_{cav}\rangle + \langle P\rangle}{\omega_{cav}} = ig(\langle\sigma_{12}a^\dagger\rangle - \langle\sigma_{21}a\rangle) \tag{39}$$

with the boundary that $\omega_h = \omega_c + \omega_{cav}$, the sum of the heat currents and the power is zero. therefore, the equations of motion fulfill the equations of motion. . With the results for σ_12 from the high f approximation, we get the results for the photocurrent and the power. The approximated result for the photocurrent with (12)

$$\langle J_{cav}\rangle = 2\omega_{cav}\Big(n_{cav} - \frac{2fg\mathrm{Re}[\sigma_{12}] + f^2}{\kappa}\Big), \tag{40}$$

and the power

$$P = 2\omega_{cav}\frac{fg\mathrm{Re}[\sigma_{12}] + f^2}{\kappa}. \tag{41}$$

Note that the approximate formulas (37),(38),(40),(41) together yield the first law of thermodynamic With the formulas (33) and (34) we can express the heat current as follow:

$$\langle J_h\rangle = -\frac{4f^2g^2\gamma_c\gamma_h(-n_c+n_h)\omega_h}{\gamma_c\gamma_h\kappa^2(\gamma_cn_c+\gamma_hn_h)(n_c+n_h+3n_cn_h)+4f^2g^2(\gamma_c(2+3n_c)+\gamma_h(2+3n_h))}, \tag{42}$$

and

$$\langle J_c\rangle = \frac{\langle Jh\rangle}{\omega_h}\omega_c. \tag{43}$$

An important aspect that is intended to be demonstrated by the figure 3 is the adherence to the first law of thermodynamics. The black line represents the sum of heat flow, photon flow, and power. A constant at zero is observed. That is also a good sanity check for us. The other main statement of Fig 3 is saturation, where the heat currents J_h and J_c initially start from zero. As the coupling strength g increases, the three-level system interacts with photons, preventing the occurrence of photocurrent and hindering the initiation of the described cycle. However, with an increased g, the cycle can gradually establish the heat currents J_h and J_c. If the cavity maintains a constant coherent field with a strength f, there exists a current between energy levels E_1 and E_2 even without coupling. The stimulation emission effect from the external field accelerates the increase in heat current.

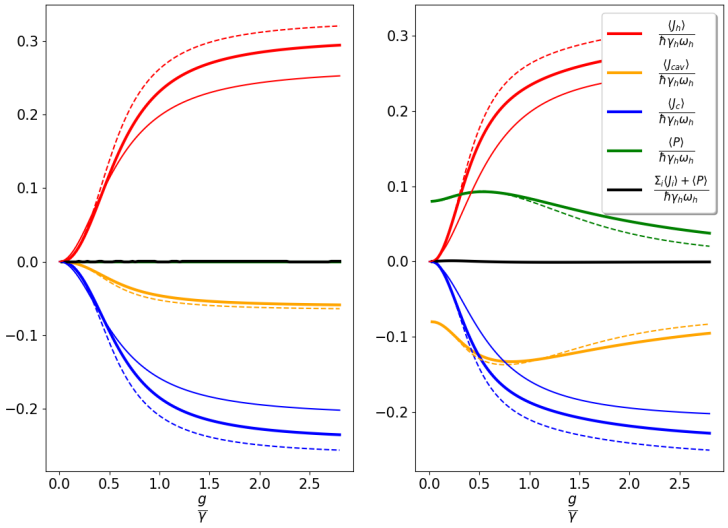

Figure 3: The heat currents calculated with (33)-(35) and the power (36) are calculated against different coupling constants g. With thick solid lines, the numerical calculations are visualized. The high f approximation is shown with thin solid lines Dashed lines show the results of the equations of motion. The temperature $n_h = 11$ is set to the maximum in entropy production. The parameters for the system are, expressed with the decay rates $\gamma = 1$. The values for all the relevant parameters in the system are $\gamma_c = \gamma_h = gamma = 1, g = 14\kappa, \omega_{cav} = 30\gamma, \omega_h = 150\gamma, \omega_c = 120\gamma, n_h = 11, n_c = n_{cav} = 0.01, \kappa = 0.2\gamma$. The left figure shows the results for the $f = 0$ case. The right figure shows the $f = 0.2$ case.

6.2 Second law

Another important concept in thermodynamics is entropy, which describes the measure of irreversibility. The change in entropy ΔS is determined by the change in heat ΔQ and the temperature change. This relationship is given by:

$$\Delta S = \sigma - \frac{Q}{T} \tag{44}$$

According to the second law of thermodynamics, for an isolated system, the entropy always remains the same or increases but never decreases. In terms of instantaneous quantities, this principle can be expressed through the entropy production rate $\dot{\sigma}$, which should always be greater than or equal to zero:

$$\dot{\sigma} \geq 0 \tag{45}$$

Since our focus is on steady-state quantities, we can calculate the entropy production rate by summing up the contributions from heat flow (33)-(35) divided by the respective bath temperature. The formula for the entropy production rate in the steady state is:

$$\dot{\sigma} = k_B \partial_t S[\rho_S] - \left(\frac{J_c}{T_c} + \frac{J_h}{T_h} + \frac{J_{cav}}{T_{cav}} \right), \tag{46}$$

where S is the von Neumann Entropy.

The entropy production rate for different values of n_h is plotted in Figure 4. We observe a distinct maximum at $n_h \approx 11$. The contribution to the entropy production rate from the hot bath is smaller compared to the contribution from the cold bath. This is because the hot bath temperature is much higher, resulting in a smaller value of $\sigma = \frac{J_h}{T}$ compared to the entropy production rate of the cold bath. By increasing the external field we see an increased entropy production rate. Overall a similar behavior as described in 7 is visible.

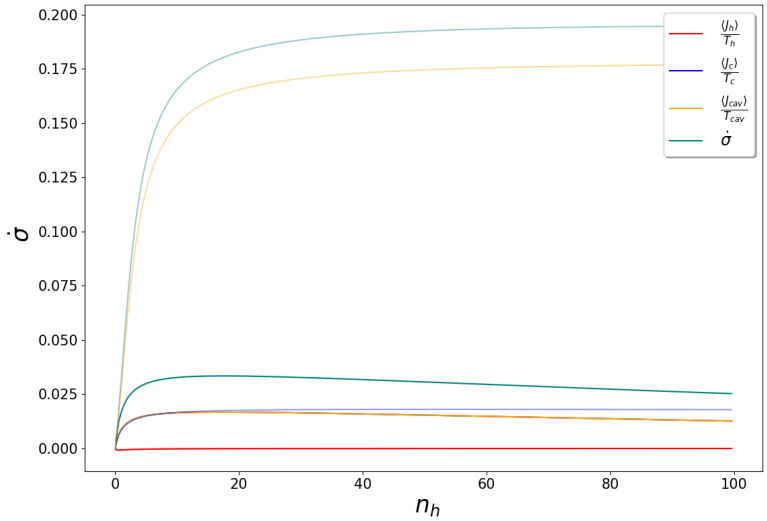

Figure 4: The entropy production for different n_h is shown in this figure. The heat currents calculated with (33)-(35) and the power (36) are calculated against different Bose-Einstein distributions nh_h. With thick solid lines, the numerical calculations are visualized. Dashed lines show the results of the equations of motion. The temperature $n_h = 11$ is set to the maximum in entropy production. The parameters for the system are, expressed with the decay rates $\gamma = 1$. The values for all the relevant parameters in the system are $\gamma_c = \gamma_h = \gamma = 1, g = 14\kappa, \omega_{cav} = 30\gamma, \omega_h = 150\gamma, \omega_c = 120\gamma, n_c = n_{cav} = 0.0, \kappa = 0.2\gamma$

7 Double threshold behavior and population inversion

The population inversion can be determined by calculating the probability of the occupation of different states $Tr[|i\rangle\langle i|\,\rho]$, where i represents the different occupation levels. When we increase the temperature n_h the population of state $|2\rangle$ (P2) is higher than the population of state $|1\rangle$ (P1), we observe a population inversion. It is shown in 6.
This phenomenon is crucial for lasing to occur, as it requires a threshold level of emission. However, if the heat flow is increased excessively, the system will produce thermal light instead of lasing, resulting in a double threshold behavior.

To investigate this double threshold behavior, we analyze the steady state of the cavity coupled to the three-level system. This behavior can be explained by the Zeno effect, which suggests that rapid successive measurements can prevent the transition from one state to another. Similarly, when sufficient stimulation is applied quickly, the system exhibits similar behavior.

When the hot bath (n_h) temperature is relatively low ($n_h \approx n_c$), the heat current is low as well and the level E_1 is most occupied. As the temperature increases, a population inversion occurs6, leading to an increase in the photon current 5 and the output of the light state resembling a state of light that looks similar to a PHAV state 7.1 7. However, when the temperature becomes too high, the average photon number decreases again, indicating a double threshold behavior. In this case, the excitation is too weak, and the system is considered to be below the lasing threshold, producing output light similar to a thermal state. In fig. 5 the heat current and the power are plotted against the temperature. The left figure show the heat current without an external field and the right figure with a field. We see a double threshold behavior in the heat current. The impact of the field for the heat currents J_h and J_{cav} is visible for high temperatures. But the field has a bigger influence on the photocurrent J_{cav}. It is apparent, that the values of the curve with a small external field coincide with the curve without an external field, until the maximum heat current. After this maximum, the heat current without the field decreases much faster. An explanation for that is, that the occupation probability in the case of an existing external field $P2$ doesn't saturate for high temperatures (high n_h). An explanation is that the external field ensures through stimulated emission, that the P_2 doesn't saturate. The effect that the external field has could be used for better advantage in heat currents or to distinguish if the actual temperature is before or after the double-threshold behavior. Further, it can be used to determine which region of temperature we are in. Therefore you can use the difference between the heat current with and without an external field to make conclusions about the temperature.

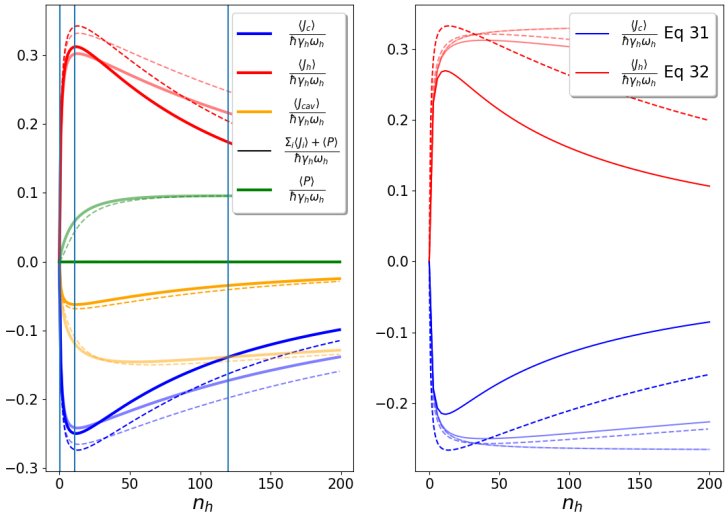

Figure 5: The heat currents calculated with (33)-(35) and the power (36) are calculated against different Bose-Einstein distributions nh_h. With thick solid lines, the numerical calculations are visualized. Dashed lines show the results of the equations of motion. The temperature $n_h = 11$ is set to the maximum in entropy production. The parameters for the system are, expressed with the decay rates $\gamma = 1$. The values for all the relevant parameters in the system are $\gamma_c = \gamma_h = \gamma = 1, g = 14\kappa, \omega_{cav} = 30\gamma, \omega_h = 150\gamma, \omega_c = 120\gamma, n_c = n_{cav} = 0.0, \kappa = 0.2\gamma$. The high f approximation is shown with thin solid lines in the figure. The non-transparent line shows the $f = 0.2$ case. With semi-transparent lines are the calculations for $f = 0.7$ and visualized the $f = 28$ case.

So far, this work has predominantly focused on the effects of a small external field. However, how does the situation change when the strength of the external field f is significantly larger than g?

We aim to investigate the consequences when the strength of the external field f is ten times greater than the coupling constant g. Due to the numerical complexity of statements regarding the applications of an external field, the plot **??** displays only the solutions of the numerically solved equations and the functions of heat flow for the high f approximation (42) and (43).

Observing the plot 5.2 on the right, we notice a rapid increase in heat flow with rising temperature. Nevertheless, the curve plateaus at the magnitude of the double-threshold behavior's peak and remains constant.

In comparison to plot 5, one could argue that the external field counteracts the double-threshold behavior. There is no longer a decrease in heat flow for high temperatures.

Analytically, the photon current and power are now dependent only on f^2 and are no longer influenced by n_h. Hence, we observe constancy in the plot on the left.

7.1 Wigner functions for different temperatures

When we look at the Wigner plots is remarkable that by no external field, we have a state that is similar to a phase average coherent state (PHAV) [1]. We plot the Wigner functions for zero temperature $n_h = 0.1$ where we see something similar to a vacuum state. If we increase the temperature, the size of the ring increases as well. The largest ring from the PHAV state we find after the peak of the double threshold behavior at $n_h = 11$. After reaching the peak, by increasing the temperature further, the PHAV state disappears and goes into a thermal state. We see these phenomena at the Wigner plot for $n_h = 120$

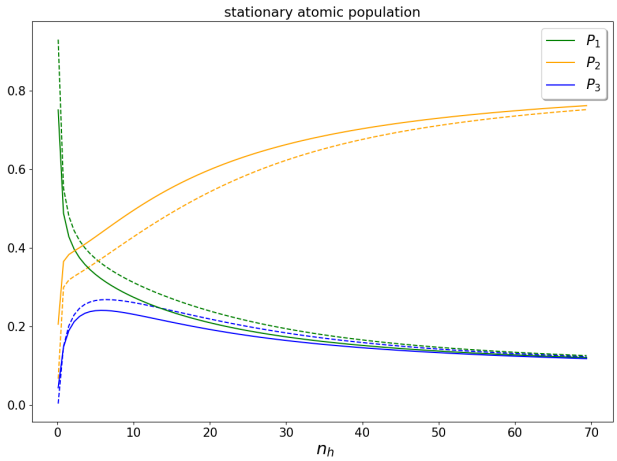

h

Figure 6: The probability for an atom to stay in a state $|1\rangle, |2\rangle$ or $|3\rangle$ vs n_h. The temperature $n_h = 11$ is set to the maximum in entropy production. The parameters for the system are, expressed with the decay rates $\gamma = 1$. The values for all the relevant parameters in the system are $\gamma_c = \gamma_h = gamma = 1$,$g = 14\kappa, \omega_{cav} = 30\gamma, \omega_h = 150\gamma, \omega_c = 120\gamma, n_h = 11, n_c = n_{cav} = 0.02, \kappa = 0.2\gamma$..

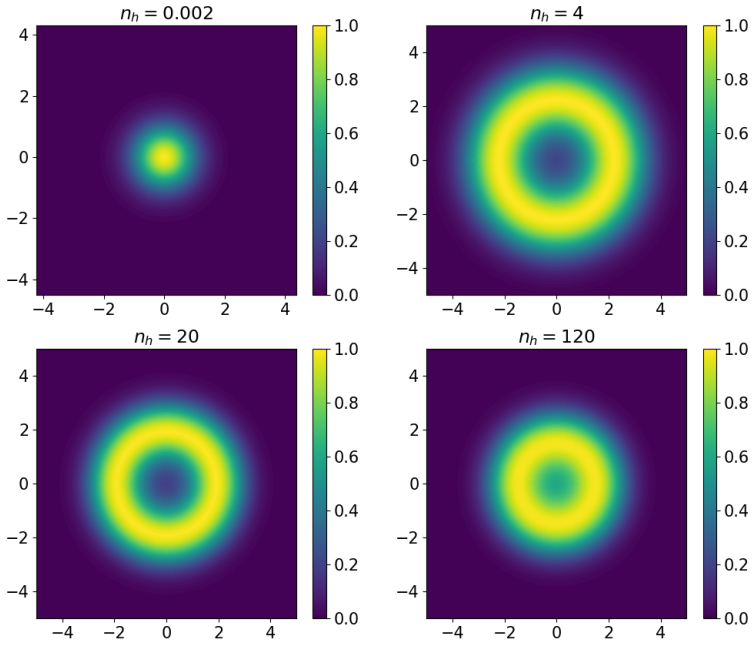

Figure 7: The Wigner functions for four different temperatures. Those temperatures are marked with a blue line in the fig 5. The parameters for the system are, expressed with the decay rates $\gamma = 1$. The values for all the relevant parameters in the system are $\gamma_c = \gamma_h = gamma = 1$,$g = 14\kappa, \omega_{cav} = 30\gamma, \omega_h = 150\gamma, \omega_c = 120\gamma, n_h = 11, n_c = n_{cav} = 0.02, \kappa = 0.2\gamma$.

8 Influence of the external field

8.1 Photocurrent and Power

We are highly interested in the performance and the effective power of thermal heat engines. An external field induces power in the process. However, our primary focus is on effective performance. Consequently, we are analyzing the difference between the photon current and the overall power. Without an external field, this corresponds directly to the photon current. With the external field, we observe a difference that peaks at the double-threshold behavior.

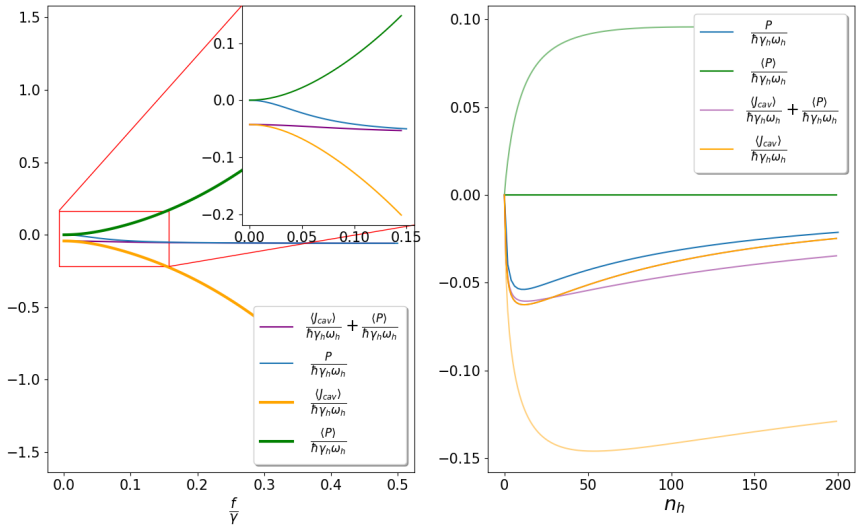

[h]

Figure 8: On the left figure the heat currents J_{cav} (35) as well as the power (36) are visualized with solid, non-transparent lines and the power against different values of the temperature n_h. The temperature $n_h = 11$ is set to the maximum in entropy production. The parameters for the system are, expressed with the decay rates $\gamma = 1$. The power draw with the light blue line shows the power out of the paper [4] The values for all the relevant parameters in the system are $\gamma_c = \gamma_h = gamma = 1, g = 14\kappa, \omega_{cav} = 30\gamma, \omega_h = 150\gamma, \omega_c = 120\gamma, n_h = 11, n_c = n_{cav} = 0.02, \kappa = 0.2\gamma$ On the right figure, the calcultations are made for different n_h.

We obsorve, that for a strong external field, we get the same power output as in [4]. For weak external field we get evenmore power out of the system.

8.2 Non-linear behavior from the field

Out of (12), we conclude that for the zero temperature $n_h = 0$ our system behaves like a two-level system. Out of the observables in the work [2] we conclude, that their results are related to our equation of motion. In their work, they obtain the result of the $\langle\sigma_{12}\rangle$ with adiabatic elimination. They yield the result:

$$\langle\sigma_{12}\rangle = \frac{f}{(2f^2 g + g^3)} \tag{47}$$

If we plug the result for $\langle\sigma_{12}\rangle$ into the equation for $\langle a\rangle$, the following result can be extracted:

$$\langle a\rangle = \frac{-i(g\langle\sigma_{12}\rangle + f)}{\kappa} = \frac{-if^3}{g^2 + 2f^2}\kappa \tag{48}$$

To understand the cubic behavior of the system, we look at the Taylor series. Remarkably, the third-order term smallest order term

$$\langle a\rangle \approx -\frac{2if^3}{g^2\kappa} + \mathcal{O}(f^5) \tag{49}$$

This f^3 behavior ensures that it needs a strong field and that the photocurrent is unequal to zero by zero temperature. The cubic behavior is seen in the following plot:

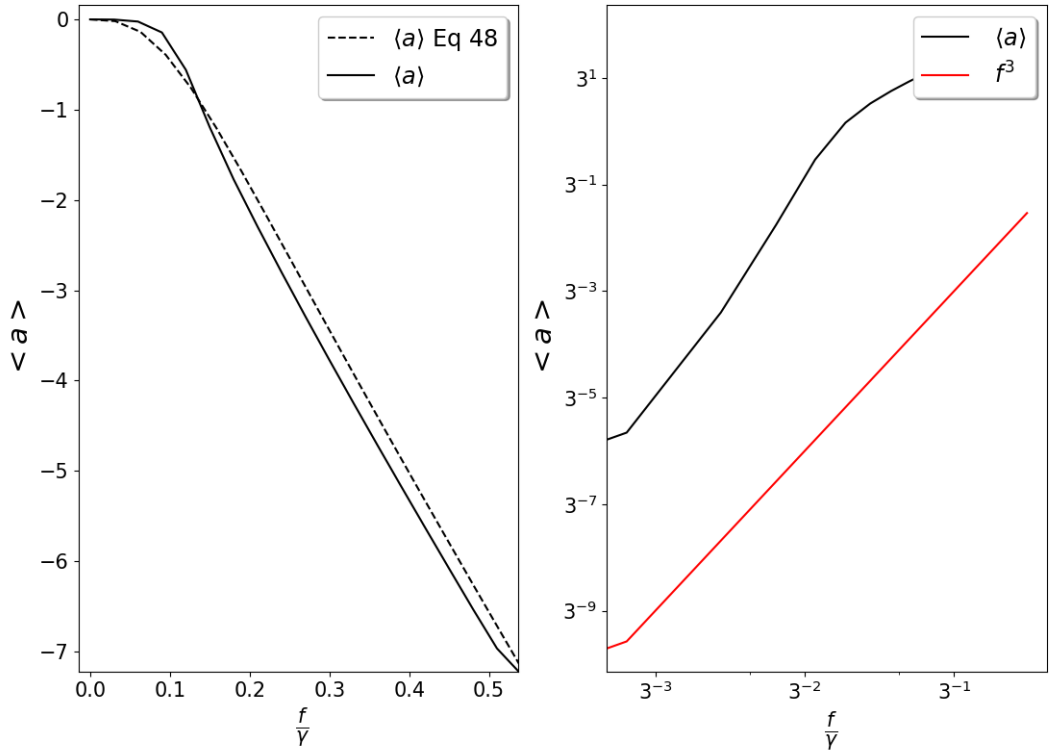

Figure 9: On the left side, the expected value of a is plotted, once numerically with a solid line and once using the analytically derived formula from Aufleres' paper [2]. On the right side, a logarithmic plot is shown, which plots the numerically calculated value logarithmically to the base three. In red, f^3 is plotted to provide a reference line. The parameters for the first plot are $n_c = 0.02, , n_h = 0, n_f = 0.02, \kappa = 0.07, g = 2.8\gamma$.

8.3 Wigner function as a function of external field strength, f

By injecting a coherent external field, the state PHAV combines with the coherent state to a combination where the probability density relocates from a homogenate ring more and more into one site until it has this banana shape. If we truncate the external field more we see a coherent state instead of a PHAV state.

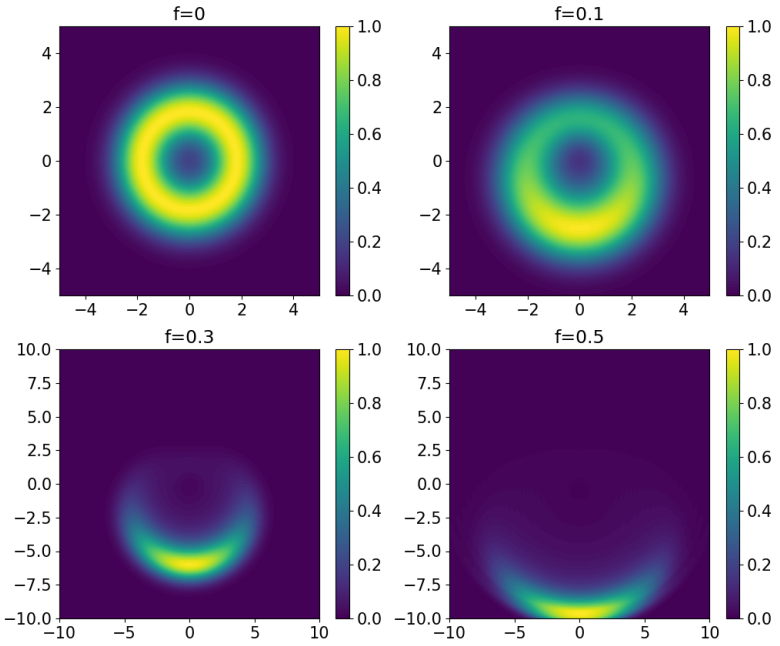

[H]

Figure 10: The Wigner functions for four different field strengths f. Those temperatures are marked with a blue line in the figure 2. The temperature $n_h = 11$ is set to the maximum in entropy production. The parameters for the system are, expressed with the decay rates $\gamma = 1$. The values for all the relevant parameters in the system are $\gamma_c = \gamma_h = \gamma = 1, g = 14\kappa, \omega_{cav} = 30\gamma, \omega_h = 150\gamma, \omega_c = 120\gamma, n_h = 11, n_c = n_{cav} = 0.02, \kappa = 0.2\gamma$.

Considering the photon current and power, it is observed that neither the power nor the photon current exists when an external field exists that matches the temperature of the hot bath to the temperature of the cold bath. This behavior only disappears when the external field is huge compared to g. At a certain sufficiently large value of f, we also have a photon current without any temperature difference between the baths. Therefore, there is a cubic behavior value for f that must be exceeded for the expectation value of the lowering operator to be non-zero. This also makes the equation for power (36) non-zero. The explanation for this behavior is described in the paper from [2] where they provide exhibits of a giant optical nonlinearity due to the saturation of the two-level system at very low intensities, of the order of one photon per lifetime.

9 Fluctuation theory

In this section we want to know more about the system and the variance of the current, to have a view of the variation of the current and the Thermodynamic Uncertainty Relation.

9.1 Thermodynamic Uncertainty Relation

The Thermodynamic Uncertainty Relation (TUR) is a fundamental inequality that relates the fluctuations of different thermodynamic quantities in a quantum system. It provides a limit on the precision with which certain pairs of thermodynamic variables can be simultaneously measured in the presence of quantum fluctuations.

$$\frac{\dot{\sigma}}{2} \geqslant \frac{\langle J_h \rangle^2}{\mathrm{Var}(J_h)} \tag{50}$$

The derivation comes directly out of the second law [3]. The uncertainty relation itself is derived from Cramér-Rate function.

If the TUR is violated, it implies that the system is operating outside the bounds of classical thermodynamics and that quantum effects are significant. Violations of the TUR have been observed in various quantum systems, such as several quantum heat engines. The TUR provides insights into the fundamental limits of precision in thermodynamic measurements in the quantum regime. It highlights the trade-off between the accuracy of heat and entropy measurements and the impact of quantum fluctuations on these measurements. to look into the TUR.

9.2 Full counting statistics

Full counting statistics refers to a mathematical framework that describes the statistical properties of counting processes, such as the number of particles or events occurring in a given system. It covers a comprehensive analysis of the probability distribution, in our case the density matrix, of counting events, including the variance.do no s chi und rho vo chi usfiehre The formalism of full counting statistics is based on moment-generating functions and their derivatives, similarly laid out as the generating field in Quantum Field theory encodes the statistical properties of the counting process. By manipulating these generating functions, one can extract valuable information about the system, such as the average current, the variance, and the noise. The moment-generating function is,

$$M(\chi, t) = \mathrm{Tr}\{e^{\mathcal{L}_\chi t}\rho\} \tag{51}$$

with the tilted liouvillian which satisfies the following equation

$$\frac{\partial \rho_\chi}{t} = \mathcal{L}_\chi \rho_\chi(t) \tag{52}$$

Where,

$$\rho(\chi) = \sum_i^\infty e^{it\chi}\rho(n) \tag{53}$$

with $\rho(n)$ the resolved density matrix Overall, full counting statistics provides a powerful tool for understanding and quantifying the statistical behavior of counting processes in various physical systems, ranging from quantum transport to stochastic processes in classical systems. Its applications have proven to be crucial in fields such as quantum mechanics

To check the thermodynamic uncertainty relation we choose the variance of the current J_h, which could be calculated in general with the two-point correlation function, or in our cases with stochastical

moments. The n-th moment of a random variable is defined as the expected value of the n-th power of the random variable. As in [5] we need a moment generating function for the current J_h to investigate the variance of our system.

In our specific case, if we analyze the heat current, the Liouvvilion transforms into the form:

$$\mathcal{L}(\chi) = e^{i\chi\nu_1}\frac{\gamma_h}{2}(n_h+1)\sigma_{31}\rho\sigma_{31}^\dagger - \{\sigma_{31}^\dagger\sigma_{31},\rho\} + e^{i\chi\nu_2}\frac{\gamma_h}{2}(n_h)\sigma_{31}\rho\sigma_{31}^\dagger - \{\sigma_{31}^\dagger\sigma_{31},\rho\} + \mathcal{L}_c + \mathcal{L}_{cav} \tag{54}$$

The partial derivative with respect to χ from $\mathcal{L}(\chi)$ correspondent to the current and therefore we introduce a new superoperator $\mathcal{J}$,

$$\mathcal{J}\rho = \partial_\chi\mathcal{L}(\chi)\rho|_{\chi=0} = \nu_1\frac{\gamma_h}{2}(n_h+1)(\sigma_{13}\rho\sigma_{13}^\dagger) + \nu_2\frac{\gamma_h}{2}(n_h)(\sigma_{31}\rho\sigma_{31}^\dagger). \tag{55}$$

It is also possible to express the heat current $\mathrm{Tr}\{H_{free}\mathcal{L}_h\rho\} = \mathrm{Tr}\{J\rho\}$ The $\tau = 0$ case can be described by introducing K which looks as follow,

$$K = \partial_\chi^2\mathcal{L}(\chi)\rho|_{\chi=0} = \mathrm{Tr}\left\{\nu_1^2\frac{\gamma_h}{2}(n_h+1)\sigma_{13}\rho\sigma_{13}^\dagger + \nu_2^2\frac{\gamma_h}{2}(n_h)\sigma_{31}\rho\sigma_{31}^\dagger\right\}. \tag{56}$$

For more information about the calculation with tilted Liouvillian look in[5]. The variance $D(t)$ is then given as

$$D(t) = -\mathrm{Tr}\left\{\partial_\chi^2\mathcal{L}\rho\right\} - 2\,\mathrm{Tr}\{\partial_\chi\mathcal{L}\partial_\chi\rho_\chi\} - 2\,\mathrm{Tr}\{\partial_\chi\mathcal{L}\partial_\chi\rho_{chi}\}, \tag{57}$$

with

$$\partial_\chi\rho_\chi = \int_0^\infty d\tau e^{\mathcal{L}(r-\tau)\partial_\chi\rho(\tau)}. \tag{58}$$

In order to implement the variance in a numerically efficient way, vectorization was used here in the implementation of the equation (57). further details are in the appendix C.1

9.3 Violating the TUR

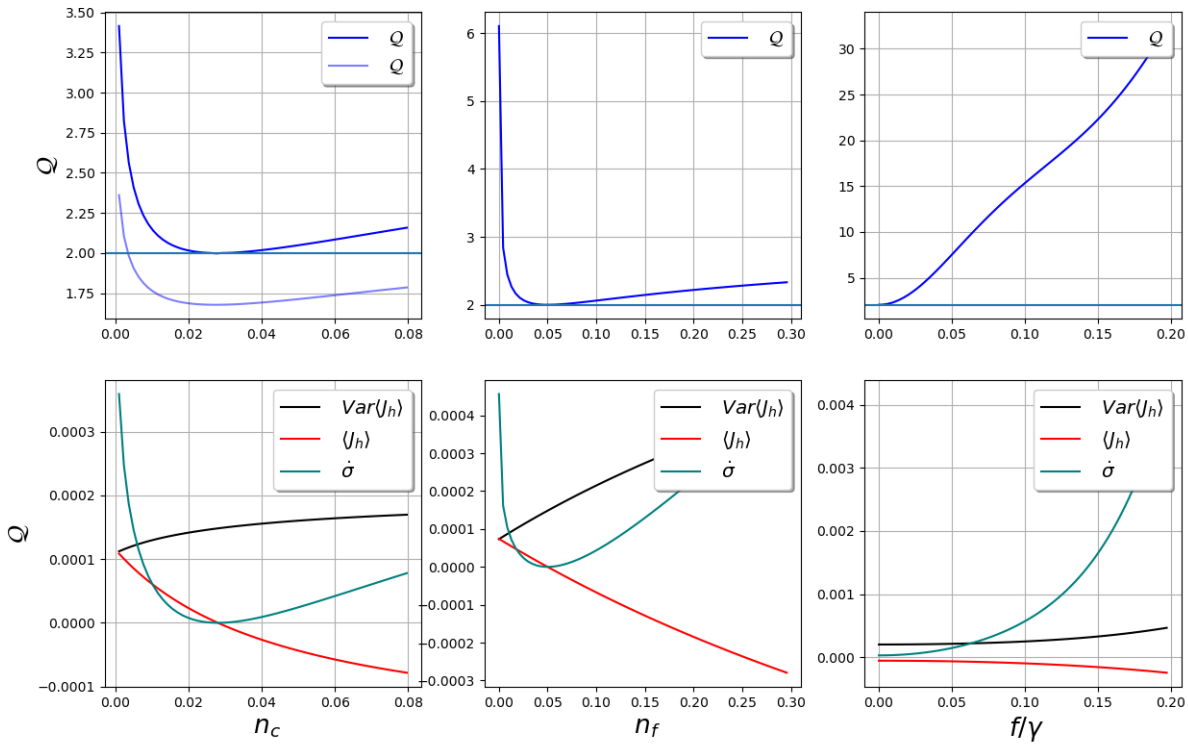

Figure 11: The Energys of the levels of the system are $\omega_1 = 0, \omega_2 = 30, \omega_3 = 150$, The reduced plank constant $\hbar = 1$ and the Bolzman constant $k_B = 1$ The temperatures are $n_h = 5, n_c = 0.027 n_f = 0.07$, The decay rates from the atomic transitions are $\gamma_h = 0.1\gamma_c = 2$ The decay rate from the cavity is $\kappa = 0.002$, the coupling constant is $g = 2.8$. The external field is set to zero $f = 0.00010714$. The $\mathcal{Q}$ draw with the light blue line shows the power out of the paper [4]

To visualize the TUR violation the formula is reformed to $\mathcal{Q} = \dot{\sigma} \frac{Var\langle J \rangle}{\langle J \rangle^2} k$ To examine for which parameter the TUR is violated, it is necessary to look at the coupling constant g, the strength of the field f, and the temperatures n_h, n_c, and n_f. In the first figure where n_c is plotted, it is remarkable that the TUR is only violated for small temperatures. This work by e einstein occupation number between $(0.2 < n_h < 5)$. This is understandable, as the entropy production and variance increase enormously at higher temperatures. What is surprising, however, is that the TUR is only violated below the peak of the double threshold. The blue line represents the $\mathcal{Q}$ as plotted in the paper [4]. We observe that under these conditions, fewer TUR violations occur, but the curve behaves similarly. The parameters, which also exist in [4], are the same; however, the Hamiltonian in my system differs from that presented in this paper. We observed the better TUR violation for small κ. Interestingly, the TUR is violated at most before the peak of the double-threshold behavior. After reaching the peak of Double-threshold behavior, the state turns more and more into a thermal state. We can assume through our observation, that a thermal state doesn't violate the TUR.

To better visualize the effect of detuning, it is necessary to activate the external field. To capture the behavior effectively for small deviations, I opted for a large field of $f = 0.2$. Under these conditions, there is no longer any violation of the TUR. However, it is evident that even a slight detuning leads to a reduced TUR violation.

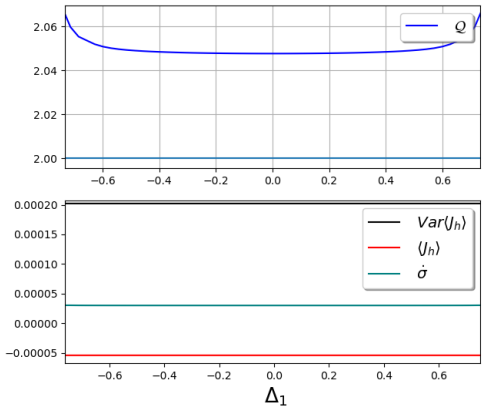

Figure 12: The Energys of the levels of the system are $\omega_1 = 0, \omega_2 = 30, \omega_3 = 150$, The reduced plank constant $\hbar = 1$ and the Bolzman constant $k_B = 1$ The temperatures are $n_h = 5, n_c = 0.027 n_f = 0.07$, The decay rates from the atomic transitions are $\gamma_h = 0.1\gamma_c = 2$ The decay rate from the cavity is $\kappa = 0.002$, the coupling constant is $g = 2.8$. The external field is set to zero $f = 0.00010714$.

When looking at the influence of f Fig b) on the variance, it is noticeable that the variance slowly decreases as the external field increases. However, the total entropy production increases enormously, which is why it is no longer violated at higher external fields. The best results we get are by the absence of the external field.

During the examination of the coupling constant, it is remarkable that $\mathcal{Q}$ decreases with increasing temperature until below 2. Therefore we need a high coupling constant for the quantum behaviour.

10 Conclusion

In my thesis, we identified various quantum properties of the heat flow as a function of temperature n_h, external field f, and coupling constant g. We observed a double-threshold behavior in the heat flow. Increasing the external field or coupling constant also led increase in the heat flow. When increasing g we observed saturation of the heat current, while increasing the field resulted in a quadratic increase without any saturation behavior. When considering the influence of the temperature of the hot reservoir, we observed a double-threshold behavior when turning on and off the external field. We found that the heat flow changes more or less depending on the temperature when an external coherent field, without detuning, is turned on or off. Thus, conclusions about the temperature can be drawn from observing the heat flow. We also showed that it is possible to calculate the average behavior of the respective observables using equations of motion. However, approximations are needed to solve these equations of motion. In this thesis, we also examined the heat flow of the Scovil-Schulz-DuBois thermal power machine concerning thermodynamic uncertainty Q. It is important to mention that the heat flow behaves very similarly to power, and statements about power can be made by considering the heat flow. From numerical calculations, it is evident that the coherent field exhibits a quantum advantage compared to its classical counterpart when detuning is small. In cases with a large quantum advantage, the maser has a smaller limit than the conventional TUR limit $\mathcal{Q} > 2$. We also demonstrated that this 3-level maser violates quantum TUR with adjusted parameters. While quantum advantages and disadvantages compared to classical systems are related to quantum-coherent dynamics, as shown in the case of heat flow, there is no direct relationship between the behavior of steady-state coherence and thermodynamic uncertainty. This is because thermodynamic uncertainty depends on the variance of heat flow, whose properties are not fully imprinted in the system's state, unlike the mean value. Thus, the introduction of an external field is necessary.

References

[1] Alessia Allevi et al. "Characterization of phase-averaged coherent states". In: *Journal of the Optical Society of America B* 30.10 (2013), p. 2621. ISSN: 0740-3224. DOI: 10.1364/josab.30.002621. arXiv: 1302.2011.

[2] Alexia Auffèves-Garnier et al. "Giant optical nonlinearity induced by a single two-level system interacting with a cavity in the Purcell regime". In: *Physical Review A - Atomic, Molecular, and Optical Physics* 75.5 (2007), pp. 1–16. ISSN: 10502947. DOI: 10.1103/PhysRevA.75.053823. arXiv: 0610172 [quant-ph].

[3] Todd R. Gingrich et al. "Dissipation Bounds All Steady-State Current Fluctuations". In: *Physical Review Letters* 116.12 (2016), pp. 1–5. ISSN: 10797114. DOI: 10.1103/PhysRevLett.116.120601. arXiv: 1512.02212.

[4] Alex Arash Sand Kalaee, Andreas Wacker, and Patrick P. Potts. "Violating the thermodynamic uncertainty relation in the three-level maser". In: *Physical Review E* 104.1 (2021), pp. 1–6. ISSN: 24700053. DOI: 10.1103/PhysRevE.104.L012103. arXiv: 2103.07791.

[5] Gabriel T. Landi et al. "Current fluctuations in open quantum systems: Bridging the gap between quantum continuous measurements and full counting statistics". In: (2023), pp. 1–59. arXiv: 2303.04270. URL: http://arxiv.org/abs/2303.04270.

[6] Sheng Wen Li et al. "Quantum statistics of a single-atom Scovil-Schulz-DuBois heat engine". In: *Physical Review A* 96.6 (2017), pp. 1–10. ISSN: 24699934. DOI: 10.1103/PhysRevA.96.063806. arXiv: 1710.00902. URL: http://arxiv.org/abs/1710.00902http://dx.doi.org/10.1103/PhysRevA.96.063806.

[7] Takahiro Sagawa. "Quantum Thermodynamics". In: *SpringerBriefs in Mathematical Physics* 16 (2022), pp. 89–115. ISSN: 21971765. DOI: 10.1007/978-981-16-6644-5_8. arXiv: 1305.2268.

[8] Murray Sargent, Marlan O. Scully, and Willis E. Lamb. *Laser physics*. 2018, pp. 1–432. ISBN: 9780429962066. DOI: 10.1201/9780429493515.

[9] H. E.D. Scovil and E. O. Schulz-Dubois. "Three-level masers as heat engines". In: *Physical Review Letters* 2.6 (1959), pp. 262–263. ISSN: 00319007. DOI: 10.1103/PhysRevLett.2.262. URL: https://link.aps.org/doi/10.1103/PhysRevLett.2.262.

[10] Xiaodan Zhang and Xingping Sheng. "Two methods for computing the Drazin inverse through elementary row operations". In: *Filomat* 30.14 (2016), pp. 3759–3770. ISSN: 03545180. DOI: 10.2298/FIL1614759Z.

A Rotating frame transformation

In this section of the appendix, our focus is on the transformation of the master equation into the rotating frame. To derive the master equation with the density matrix in the rotating frame, we begin by multiplying out the chain rule from the left side of the equation. As a result, we observe the emergence of two new terms in the equation.

$$
\begin{aligned}
&i\partial t\rho_I = (\partial_t U^\dagger)\rho U + U^\dagger(\partial_t\rho)U + U^\dagger\rho(\partial_t U)\\
&= (\partial_t U^\dagger)\rho U + U^\dagger(-i[H,\rho] + \sum_i \gamma_i 2A_i\rho A_i^\dagger - A_i^\dagger A_i\rho - \rho A_i^\dagger A_i)U + U^\dagger\rho(\partial_t U)\\
&= \partial_t U^\dagger\rho U + U^\dagger\rho\partial_t U - i(U^\dagger HUU^\dagger\rho U - U^\dagger\rho UU^\dagger HU)\\
&+ \sum_i \gamma_i 2U^\dagger A_i UU^\dagger\rho UU^\dagger A_i^\dagger U - U^\dagger A_i^\dagger UU^\dagger A_i UU^\dagger\rho U\\
&- U^\dagger\rho UU^\dagger A_i^\dagger UU^\dagger A_i U)\partial_t U^\dagger UU^\dagger\rho U + U^\dagger\rho UU^\dagger\partial_t U - i[U^\dagger HU,\rho_I]\\
&+ \sum_i \gamma_i 2(U^\dagger A_i U)\rho_I(U^\dagger A_i^\dagger U) - (U^\dagger A_i^\dagger U)(U^\dagger A_i U)\rho_I
\end{aligned}
\tag{59}
$$

In the first line is the chain role from the partial derivation of the density matrix.
Then the chain role acts on the right part of the master equation.
In the third line, the commutator is written out.

In the beginning, the focus is on the unitary part of the master equation.
To truncate the equation the property $\mathbb{1} = U^\dagger U$ is used. We get:

$$\begin{aligned} i\partial t\rho_I &= -i(U^\dagger HU + i\partial t U^\dagger U)\rho_I + i\rho_I(U^\dagger HU + i\partial t U^\dagger U) \\ &+ \sum_i \gamma_i \mathcal{D}[U^\dagger A_i U]\rho_I \\ &= -i[(U^\dagger HU + i(\partial_t U^\dagger)U, \rho_I] + \sum_i \gamma_i U^\dagger \mathcal{D}[A_i]U\rho_I \end{aligned} \tag{60}$$

Therefore the new Hamiltonian for the rotating frame has to be:$H_I = U^\dagger HU + i(\partial t U^\dagger)U$

Transformation of the operators to the rotating frame is listed below, the calculations come from the Baker-Campbell-Hausdorff-formula

$$\begin{aligned} U^\dagger \sigma_{12} U &= e^{-i\omega_d t}\sigma_{12} \\ U^\dagger \sigma_{21} U &= e^{i\omega_d t}\sigma_{21} \\ U^\dagger a U &= e^{-i\omega_d t} a \\ U^\dagger a^\dagger U &= e^{i\omega_d t} a^\dagger \end{aligned} \tag{61}$$

The different Hamiltonians are looking after the transformation as follows:

$$U^\dagger V U = f(a + a^\dagger) \tag{62}$$

$$U^\dagger H_{free} U^\dagger = \Delta_1 a^\dagger a + \Delta_2 |2\rangle\langle 2| \tag{63}$$

$$U^\dagger H_{int} U = g(\sigma_{12} a^\dagger + \sigma_{21} a) \tag{64}$$

It is also necessary to transform the non-unitary part of the von Neumann equation.

$$\mathcal{D}[UAU^\dagger]\rho_I = (2UAU^\dagger \rho_I UA^\dagger U^\dagger - UA^\dagger U^\dagger UAU^\dagger \rho_I - \rho_I UA^\dagger U^\dagger UAU^\dagger). \tag{65}$$

When we insert the operators A from the transformation (61) we get:

$$\mathcal{D}[UAU^\dagger]\rho_I = (2e^{-i\omega_d t} A\rho_I e^{+i\omega_d t} A^\dagger) - (e^{i\omega_d t} A^\dagger e^{-i\omega_d t} UAU^\dagger \rho_I) - (\rho_I e^{i\omega_d t} A^\dagger e^{-i\omega_d t} A). \tag{66}$$

Where A is one of the operators form (61). Because the dissipative part (61) have the therms $AA^\dagger$ the time-dependent therms of $e^{-i\omega_d t}$ and $e^{i\omega_d t}$ canceled each other out. Therefore the unitary transformation to the rotating frame has no effect $U^\dagger \mathcal{D}[A]\rho U = \mathcal{D}[A]\rho$.

B Equation of motion

In case of steady states and if the parameters Δ_1, Δ_2 are set to zero, we get out of equation (19) that

$$\mathrm{Re}[\langle\sigma_{12}\rangle] = -\frac{\mathrm{Im}[\langle a\rangle]\kappa}{g} \tag{67}$$

out of equation (19)

$$\mathrm{Im}[\langle\sigma_{12}\rangle] = \frac{\mathrm{Re}[\langle a\rangle]\kappa}{g} \tag{68}$$

Out of equation (22)

$$\mathrm{Im}[\langle\sigma_{12}\rangle] = -\frac{2\mathrm{Re}[\langle a\rangle]g\langle p_1 - p2\rangle}{n_c\gamma_c + n_h\gamma_h} \tag{69}$$

$$\frac{\mathrm{Re}[\langle a\rangle]\kappa}{g} = -\frac{2\mathrm{Re}[\langle a\rangle]g\langle p1 - p2\rangle}{n_c\gamma_c + n_h\gamma_h} \Rightarrow \mathrm{Re}[\langle a\rangle] = 0 \tag{70}$$

Out of (68) we see that also $\mathrm{Im}[\langle\sigma 12\rangle]$ have to be zero. from equation (23) follow that

$$\mathrm{Re}\langle\sigma_{12} a^\dagger\rangle = \frac{2f\mathrm{Im}\langle\sigma_{12}\rangle}{n_c\gamma_c + n_h\gamma_h + 2\kappa} => \mathrm{Re}\langle\sigma_{12} a^\dagger\rangle = 0 \tag{71}$$

The analytical result for n with the parameters $\gamma_h = \gamma_c = \gamma$

$$\begin{aligned}
\langle a^\dagger a\rangle = & \frac{1}{(8g^2(2+nc+2nh)(4+3nc+3nh)\gamma^2\kappa)}(-((2+n_c+2n_h)\gamma^2((n_c+n_h+3n_cn_h)\gamma\kappa \\
& (n_c\gamma+nh\gamma+2\kappa)+2g^2(4\kappa-8n_{cav}\kappa+nc(\gamma+2\kappa]-6n_{cav}\kappa)-nh \\
& (\gamma-4\kappa+6n_{cav}\kappa)))) \\
& +((2+n_c+2n_h)^2\gamma^4((n_c+n_h+3n_cn_h)^2\gamma^2\kappa^2(n_c\gamma+n_h\gamma+2\kappa)^2 \\
& +4g^4((n_c-n_h)^2\gamma^2+4(nc^2(1-3n_{cav}+6n_h)+n_c(2-4n_{cav}+15n_h+6n_h^2) \\
& +n_h(6+4n_h+n_{cav}(4+3n_h)))\gamma\kappa+4(2+n_c+4n_{cav}+3n_cn_{cav}+2n_h+3n_{cav}n_h)^2\kappa^2) \\
& +4g^2(n_c+n_h+3n_cn_h)\gamma\kappa(n_c\gamma+n_h\gamma+2\kappa)(-n_h\gamma+4\kappa+8n_{cav} \\
& \kappa+4n_h\kappa+6n_{cav}n_h\kappa+n_c(\gamma+2\kappa+6n_{cav}\kappa))))^{\frac{1}{2}})
\end{aligned} \tag{72}$$

The analytical solution for the occupation probability if $\gamma = 1, n_{cav}, n_c = 0$ is:

$$\begin{aligned}
\langle p_1\rangle = & -(\frac{1}{(8g^2n_h(4+3n_h))})(2+n_h)(\kappa n_h(2\kappa+n_h)+g^2(-4nh+8\kappa(1+n_h)) \\
& +\sqrt{\kappa^2nh^2(2\kappa+n_h)^2+8g^2\kappa n_h(2\kappa+n_h)(-n_h+2\kappa(1+n_h))}+ \\
& \sqrt{16g^4(n_h^2+4\kappa^2(1+n_h)^2+4\kappa nh(3+2n_h))})
\end{aligned} \tag{73}$$

$$\begin{aligned}
\langle p_2\rangle = & (\frac{1}{(4g^2n_h(4+3n_h))})(4g^2(2\kappa(1+n_h)^2+n_h(3+2n_h))+ \\
& (1+n_h)(\kappa nh(2\kappa+nh)+\sqrt{\kappa^2n_h^2(2\kappa+n_h)^2+8g^2\kappa nh(2\kappa+n_h)(-n_h+2\kappa(1+n_h))}+ \\
& \sqrt{16g^4(n_h^2+4\kappa^2(1+n_h)^2+4\kappa n_h(3+2n_h))}))
\end{aligned} \tag{74}$$

The n Operator is plotted in Fig **??** Visible is the double-threshold behavior.

C Full counting statistics

We can rewrite formula (**??**) with the fact that,

$$\langle J(t)J(t+\tau)\rangle = \langle\frac{1}{dt^2}dN(t)dN(t+\tau)\rangle \tag{75}$$

Where the new variable N is introduced, as the integrated current$N(t) = \int_0^t dt' J(t')$ In a quantum form, we can rewrite the formula above with the probability that a jump occurs P. In the next step, we calculate the average of the current, with the probability that two jumps happen at the same time from one state to another.

$$J(t)J(t+\tau) = \frac{1}{dt^2}\sum_k, q\nu_k\nu_q P(dN_k(t)=1, dN_q(t+\tau)=1), \tag{76}$$

where we used the fact that dN takes on the value ν_k whenever $dN_k = 1$. To proceed, we therefore need the joint probability $P(dN_k(t) = 1, dN_q(t+\tau) = 1)$. But to calculate the joint probability we use the conditional probability. The conditional probability with

$$\frac{d}{dt}\rho(t)\frac{dt}{p_k}\mathcal{L}_k\rho(t), \tag{77}$$

The conditional probability is now by the formula

$$P(dN_k(t)=1dN_q(t+\tau)=1) = \frac{dt^2}{p_h}\mathrm{Tr}[-\mathrm{i}[\mathrm{H},\rho]\frac{\gamma_\mathrm{h}}{2}(\mathrm{n_h}+1)\mathcal{D}[\sigma_{13}]\mathrm{e}^{\mathcal{L}\tau}\frac{\gamma_\mathrm{h}}{2}(\mathrm{n_h})\mathcal{D}[\sigma_{31}]\rho(\mathrm{t})] \tag{78}$$

The average heat current from the hot bath can then be written as :

$$\langle J_h(t)^2\rangle = \frac{1}{dt}\nu_1^2\,\mathrm{Tr}\Big\{\frac{\gamma_h}{2}(n_h+1)\sigma_{13}^\dagger\sigma_{13}\rho(t)\Big\}+\nu_2^2\,\mathrm{Tr}\Big\{\frac{\gamma_h}{2}(n_h)\sigma_{31}^\dagger\sigma_{31}\rho(t)\Big\} = \frac{1}{dt}K(t) \tag{79}$$

C.1 Vectorisation

$$vec\left(\begin{bmatrix} a & b \\ c & d \end{bmatrix}\right) = \begin{bmatrix} a \\ c \\ b \\ d \end{bmatrix} \tag{80}$$

with this vectorization, we could rewrite the Liouvillian with his eigenvectors and eigenvectors

$$\mathcal{L} = \sum_{j\neq 0} \lambda_j |x_j\rangle\!\rangle\langle\!\langle y_j| \tag{81}$$

The matrix exponential can be rewritten as

$$e^{\mathcal{L}t} = |\rho\rangle\!\rangle - \langle\!\langle \mathbb{1}| + \sum_{j\neq 0} e^{\lambda_j t} |x_j\rangle\!\rangle\langle\!\langle y_j| \tag{82}$$

now we will rewrite the two-point correlation function followed by the vectorization form and $J = \langle\!\langle \mathbb{1}|\mathcal{J}|\rho\rangle\!\rangle$:

$$\mathcal{F}(\tau) = \delta(\tau)K(t) + \sum_j e^{\lambda_j|\tau|} \langle\!\langle \mathbb{1}|\mathcal{J}|x_j\rangle\!\rangle\langle\!\langle y_j|\mathcal{J}|\rho\rangle\!\rangle \tag{83}$$

We introduce the pseudo inverse, the Drazin inverse defined as:

$$\mathcal{L}^+ = \int_0^\infty d\tau e^{\mathcal{L}\tau}(1 - |\rho\rangle\!\rangle\langle\!\langle \mathbb{1}|) = \sum_{\lambda_j\neq 0} \frac{1}{\lambda_j} |x_j\rangle\!\rangle\langle\!\langle y_j| \tag{84}$$

Where we invert the eigenvalues which are not zero for more details look in [5]

With the drazin inverse, we can rewrite equation (**??**) as follows.

$$D = K - 2\langle\!\langle \mathbb{1}|\mathcal{J}\mathcal{L}^+\mathcal{J}|\rho\rangle\!\rangle \tag{85}$$

A fast way to implement the Drazin inverse is described in the paper [10]. This approach is applicable for computing higher cumulants, whereas, for the specific task of computing variances in higher-dimensional Hilbert spaces, we have opted for a more efficient technique. In pursuit of faster implementation, we have found it advantageous to bypass the direct computation of the Drazin inverse Instead, it is faster to calculate the product of $\mathcal{L}^+\mathcal{J}|\rho\rangle\!\rangle = |z\rangle\!\rangle$ in the vectorized form directly with the following equation. The following equation with dimension $(d^2 + 1)$ is seen below:

$$\begin{pmatrix} \vdots \\ \mathcal{L} \\ \vdots \\ \langle\!\langle \mathbb{1}| \end{pmatrix} |z\rangle\!\rangle = \begin{pmatrix} \vdots \\ \mathcal{J}|\rho\rangle\!\rangle - |\rho\rangle\!\rangle\langle\!\langle \mathbb{1}|\mathcal{J}|\rho\rangle\!\rangle \\ \vdots \\ 0 \end{pmatrix} \tag{86}$$

With beneficial algebraic property

$$\mathrm{Vec}(ABC) = (C^T \otimes A)|B\rangle\!\rangle, \tag{87}$$

the calculation $\mathcal{J}|z\rangle\rangle = \sum_i^3 \nu_k(\sigma_{ij})^T \otimes \sigma_{ij}|z\rangle\rangle$, where L_k are the jump-operators. $|z\rangle\rangle = \mathcal{L}^+|\alpha\rangle\rangle$ If we solved the equation for $|z\rangle\!\rangle$, we can the next equation to get the variance $\mathrm{Var}(I) = D$ of the current.

The two superoperators $\mathcal{L}$ and $\mathcal{J}$, act on the state both on the left and right. Superoperators always act on whatever is on the right sight. Therefore superoperators behave like matrices, while ρ behaves like a vector. This connection is made precise by a procedure called vectorization and, as we will see, it leads to a significant simplification of all the formulas. It also makes their numerical computation faster. .

where D is:

$$D = K - 2\langle\!\langle \mathbb{1}|\mathcal{J}|z\rangle\!\rangle \tag{88}$$

D bullet points

1. banana-states difference between a PHAV-state and a coherent state (Wigner plot)
2. The threshold where $< a >= 0$ up to a specific value of f. Then it starts growing.(**??**)

3. The difference between the current with and without an external field. Conclude the temperature. (5)
4. The Variation of the current and the TUR. a plot from the variance and tur
5. Mention that the equations of motion matched the results from the numerics
6. Double threshold behavior from currents concerning the temperature. 5